The Impact of Model Predictive Control Structures and Constraints on a Wave Energy Converter with Hydraulic Power Take Off System

Carrie Hall, Wanan Sheng, Yueqi Wu, and George Aggidis

Abstract

Ocean waves present a promising renewable energy source, but are challenging to harness given their irregular nature. In order to maximize energy capture on wave energy converters (WECs), power take off (PTO) systems are typically used to effectively adjust the device's resonant frequency. Optimal control techniques can oversee the PTO operation to maximize overall power output, but optimization in real-time poses difficulties given the wave variability and underlying constraints of the system. This study compares two different model predictive control approaches. One method uses only a model of the hydrodynamics of the WEC while the second has a state space model that includes the WEC hydrodynamics as the dynamics of a hydraulic PTO system. The impact of the PTO constraints, control structure and control prediction horizon on the wave energy converter control performance was explored and quantified for irregular wave conditions. Results show that utilizing a model that includes both the hydrodynamics and PTO dynamics can increase power output by 23% compared to an approach that uses the hydrodynamics only.

Index Terms

wave energy conversion; power take off control; optimal control; model predictive control; constraints.

I. Introduction

As global energy demands and climate concerns continue to grow, the need for renewable energy is becoming increasingly clear. Solar and wind energy are two commonly considered renewable energy sources, but when solar energy is converted to wave energy at the water surface, the energy intensity increases [1]. This unique feature means that ocean waves could provide an excellent future energy source. Wave energy converters (WECs) have been researched for decades and much work has focused on the design of such systems. Many different structures have emerged over the years including point absorbers, attenuators, oscillating water columns and reservoirs [2]. While each of these WEC designs harnesses wave motion in a slightly different way, most designs are only able to extract energy from a single direction of motion which could limit their effectiveness. Waves cause motion over six degrees of freedom (heave, pitch, surge, roll, sway and yaw) and as such, a device that can operate over multiple axes should be able to generate more power than a single-axis devices. However, multi-axis WECs are more difficult to model and control. This is largely because the more complex motion of a multi-axis WEC causes interactions between the different motions and power absorption via the power take off (PTO) system has to take place in these different directions [3]. System constraints can also become increasingly difficult to handle as the WEC complexity increases. Over the years, several multi-axis WECs have been developed over the years including Pelamis [4] and TALOS [5] and these have the potential to harness a greater amount of wave energy. TALOS is a point-absorber type WEC with a multi-axis PTO system and control of this device will be the focus of this work. The PTO uses a heavy ball that is attached to the hull with springs and hydraulic cylinders as illustrated in Figure 1. When the hull is pushed by the external waves, the relative motion between the ball and hull moves the hydraulic cylinders causing them to pump a fluid through a circuit, thereby driving a hydraulic motor to produce electricity. This design has shown promising results in energy output but is more challenging to control since the PTO can move over six degrees of freedom.

While such multi-axis designs have potential, their PTO control can be complex. The maximum energy will be captured if the frequency of the WEC system matches the dominant frequency of the incoming wave and this is typically achieved by a PTO system that can change effectively add or remove damping and thereby affect the device frequency. A wide range of PTO systems exist including turbines, hydraulic systems, and linear actuators [6], but controlling the PTO system of a multi-axis WEC remains challenging due to the complexity of systems and the variable nature of the incoming waves. PTO systems have previously been controlled by leveraging linear models and velocity tracking, complex conjugate or impedance matching control. These approaches have been compared in [7] and [8]. While these methods have merits, they can have poor performance when operating over a wide range of conditions. Control methods that utilize optimization for PTO operation have been prevalent in recent years. A wide variety of optimal control strategies have been explored including model predictive control [9], [10], spectral and pseudospectral methods [11], [12], flatness-based [13] and moment-based approaches [14], [15]. The evolution of WEC control is discussed in more detail in [16].

Model predictive control (MPC) is a natural choice for such problems and many MPC based approaches have been investigated in recent years. Examples of MPC implementation using linear models include efforts to maximize energy from heaving wave

Fig. 1. TALOS WEC Configuration [5].

energy converters [17] and a Wavestar configuration [18] as well as experimental work with a prototype of the Azura WEC, which has shown that linear MPC can provide an average increase of 36% in power production compared to fixed damping strategies [19]. While most of the existing control efforts have leveraged linear models, linearity can be a poor assumption for a controlled WEC system since large motions can be induced that take the system outside of the equilibrium point about which it was linearized [20]. Using a nonlinear model enables better results, but nonlinear optimization can be computationally intensive. For example, nonlinear MPC has been explored for the CENTIPOD device which has two degrees of freedom and provided a 10% improvement in power output over a linear MPC approach [21].

For practical applications, MPC will need to work in real-time with wave predictions and also ensure that the control actions do not violate any constraints. If constraints are ignored, control becomes more straightforward but can lead to large motions, forces and power changes that cannot practically be achieved [22]. In reality, PTO systems will have constraints on their motion and the maximum force they can generate both for reactive and damping actions. Constraints are typically placed on the position or velocity of the WEC mass [9], but studies have also added constraints on variables related to the control input and rate of change of the control input for a generic PTO [23]–[25], direct drive PTO [26], rotary PTO [27], linear permanent magnet generator PTO [28] and hydraulic PTO [29], [30]. In many such studies, the dynamics of the PTO are not included which simplifies the solution but may result in solutions that require control responses that are not achievable.

Limits on maximum PTO power have also been introduced but make the solution more difficult [22]. Even including both force and displacement constraints can be challenging since at high excitation levels, it may be impossible to abide by all constraints [16], [31]. Iterations that have included PTO power constraints have introduced constraints on the electric motor component of a PTO [32], [33] as well as power flow and force constraints for a hydraulic PTO [34]. Efforts that have introduced constraints with PTO dynamics typically attempt to capture the dynamics via a simple loss term [35], [36]. Karthikeyan et. al examined nonlinear MPC for a flap type WEC with different hydraulic PTO configurations and constraints for PTO force. The PTO model leveraged included PTO losses and this study showed that a PTO system capable of two-way power (absorbing and reactive) produced the highest normalized annual energy output [34]. However, system model errors and wave prediction errors significantly reduced power production.

Prior studies have examined different WEC configurations and control structures, but have not examined these challenges for a WEC design with the physical motion constraints of the TALOS device. While the constraints of TALOS may limit its efficiency, it is possible that a model predictive control algorithm could improve its effectiveness since it can optimize in the presence of these constraints. MPC may in fact present more of a benefit on a constrained design like TALOS than other WEC systems and this study seeks to understand the impact of MPC on an enclosed WEC design with an inertial mass PTO. This paper examines MPC with realistic PTO and WEC motion constraints and PTO dynamics in conjunction with a nonlinear hydrodynamic model. A PTO capable of absorbing and reactive power is implemented since prior work has shown that this configuration produces a higher power output than the alternatives [34]. The work aims to guide control selection as research continues toward multi-axis WEC systems in which model complexity and constraints will become increasingly limiting as the WEC gains more degrees of freedom. Three different control approaches are explored in order to understand the influence of the model selection and the prediction horizon used for control. The primary contributions of this work are 1) contrasting the impact of including the hydrodynamics of the WEC along with PTO dynamics with the approach of using the hydrodynamics alone in the model leveraged by MPC on the power production of a WEC with an enclosed, constrained design; 2) quantifying the impact of MPC prediction horizon on power output and computational burden for such a WEC, and 3) examining the performance of these various options for sea states reflective of seasonally varying conditions at a location off the costs of Ireland and Scotland.

II. Model and Control Structure

TALOS has a main mass connected to an outer hull and can capture energy in potentially all six degrees of freedom. It is anticipated that the heave, pitch and surge motions will contain more energy and as such future work may focus the PTO on these three directions. As a step toward control in all three of these directions, a model is developed here that focuses on the heave motion and includes the hull and central ball mass motion as illustrated in Figure 2. The aim of this paper is to identify control structures that may be suitable for the TALOS device with its constraints and to understand the impact that wave prediction uncertainty plays in performance of the control algorithm.

A. Control-Oriented Model

The model includes the constrained motion between the central mass and hull as in TALOS but does not include motion in the pitch and surge directions. The simpler model will allow control structures to be identified that are suitable for the constrained TALOS system and those structures that appear most promising can be expanded to cover more degrees of freedom in further work. The masses and structure of the system have been chosen to reflect the current design of the TALOS device. In reality, the system will have hydraulic pistons both above and below the central mass, allowing for additional forces on the ball. The motion has been simplified in the model considered here to only include one piston but positive and negative PTO forces are allowed. In the real system, the PTO forces would be achieved by the upper and lower PTO elements. The motion of the central mass in TALOS is constrained by the hull and PTO elements and these constraints will be accounted for in the control approach. Once suitable control structures for this constrained system have been identified, future work will explore expansion to the full range of motion.

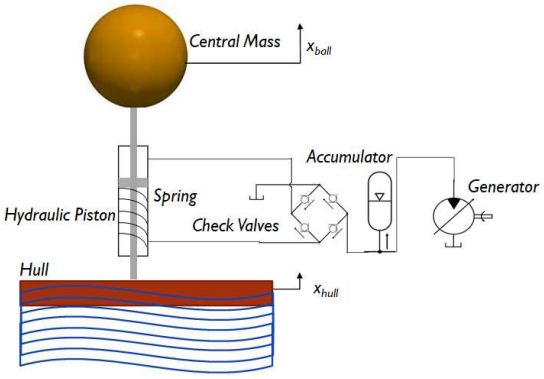

Fig. 2. Two DOF Point Absorber WEC System with Hydraulic PTO

In this system, the hull is impacted by the external wave motion and hydrodynamics while the central ball mass motion is driven by the hydraulic piston and spring action. As such, the motion of the central mass or ball is

$$M_{ball}\ddot{x}_{ball} = -f_{rest} - f_{pto} \tag{1}$$

in which M_{ball} is the mass of the central mass (in kg), $\ddot{x}_{ball}$ is the acceleration of the central mass (in m/s^2), f_{rest} is the spring force (in N), and f_{pto} is the PTO force (in N). The restoring spring force is given by

$$f_{rest} = S_{rest}(x_{ball} - x_{hull}). \tag{2}$$

where S_{rest} is the spring coefficient (in N/m), x_{ball} is the position of the central mass (in m) and x_{hull} is the position of the hull (in m).

The hydrodynamics of the hull are modeled using standard wave-structure interaction equations. Applying Newton's law to the hull, the forces acting on the body include the forces due to radiation, buoyancy, drag, and friction along with the restoring force of the spring, wave excitation force and the force generated by the PTO. Additional forces may be present such as a mooring force, but these are excluded here. The motion of the hull is captured as [17]:

$$\begin{aligned}(M_{hull} + m_{\infty,hull})\ddot{x}_{hull} = \quad & -f_{rad} - f_{buoy} - f_{drag} - f_{fric} \\ & +f_{rest} + f_{ext} + f_{pto}.\end{aligned} \tag{3}$$

in which M_{hull} is the mass of the hull (in kg), $m_{\infty,hull}$ is the added mass due to radiation (in kg), and $\ddot{x}_{hull}$ is the acceleration of the hull (in m/s^2. In Equation 3, the excitation force, f_{ext}, is taken directly from the wave prediction (discussed in Section II.D) and the PTO force, f_{PTO}, is computed via the PTO model and control action. The remaining forces include the radiation (f_{rad}), buoyancy (f_{buoy}), drag (f_{drag}) and friction (f_{fric}) forces. This base model leverages the model form used in [17].

The radiation force is captured with its own dynamic model [37] in which

$$f_{rad} = \mathbf{C}_r\mathbf{q} \tag{4}$$

and

$$\dot{\mathbf{q}} = \mathbf{A}_r\mathbf{q} + \mathbf{B}_r\dot{x}_{hull} \tag{5}$$

in which $\mathbf{q}$ represents the radiation auxiliary state vector and $\mathbf{A}_r$, $\mathbf{B}_r$, and $\mathbf{C}_r$ are the radiation state matrices. Prior work has shown that radiation forces can be expressed with such a linear model [17], [37].

The buoyancy force is given by [17]

$$f_{buoy} = \pi\rho g {R_b}^2 \left(1 - \frac{|x_{hull}|x_{hull}}{3{R_b}^2}\right) x_{hull} \tag{6}$$

in which ρ, is the density of water (in kg/m^3), g is the gravitational acceleration (in m/s^2) and R_b is the buoy radius (in m). The drag force and friction force are given by Eqs. 7 and 8, respectively, as in [17].

$$f_{drag} = 0.5\rho A_w C_d |\dot{x}_{hull} - v_f|(\dot{x}_{hull} - v_f) \tag{7}$$

$$\begin{aligned} f_{frict} = \quad & F_n\mu_d tanh(\alpha\dot{x}_{hull}) + \mu_v\dot{x} \\ & + F_n(\mu_s - \mu_d)e^{-(|\dot{x}_{hull}|/v_s)^2} tanh(\alpha\dot{x}_{hull}) \end{aligned} \tag{8}$$

In these equations A_w is the submerged surface area of the buoy (in m^2), C_d is the viscous drag coefficient, and v_f is the water surface velocity in the x direction (in m/s). The friction model assumes that viscous and Stribeck effects are present with F_n representing the normal force (in N), v_s being the Stribeck velocity (in m/s) and μ_d, μ_v, and μ_s representing the damping, viscous and static friction coefficients, respectively.

The main mass is linked to a hydraulic PTO system. Although Figure 2 only shows one PTO, the whole system (1) has multiple hydraulic PTO elements. As such, it is assumed that the PTO forces can act in both positive and negative directions since hydraulic piston assemblies will be present both above and below the main mass. A hydraulic PTO system was chosen since they are cost-effective and rely on established technology. The hydraulic PTO model is based on a previously developed state space model [38] which has been leveraged extensively for WEC PTO control studies although typically decoupled from the hydrodynamics. As illustrated in Figure 2, the system has four check valves that rectify the alternating flow of the hydraulic fluid from the piston-cylinder assembly. A gas accumulator is used to smooth the flow and the resulting flow drives a hydraulic generator producing power output. The PTO model includes the dynamics between the torque output of the generator and the force applied to the hydraulic piston. The dynamics of the underlying PTO system are often simplified and a direct link between the PTO force and power output is assumed [10], [23], [24], [39]–[41]. However, in a hydraulic PTO system this is likely a poor assumption given the anticipated delay in the dynamics. The PTO model used here includes the losses associated with the pressure drops in the pipes, motor leakage and friction. The full model derivation is detailed in [38] and results in two nonlinear differential equations that summarize the PTO dynamics. The first equation captures dynamics of the accumulator volume (V) (in m^3) by [38]

$$\dot{V} = -k_l \cdot P_a(V) - \frac{D}{J} \cdot L + S \cdot (\dot{x}_{ball} - \dot{x}_{hull}) \tag{9}$$

in which k_l is a motor leakage coefficient (in $m^5/(N \cdot s)$), $P_a(V)$ is the accumulator pressure (in Pa) posed as a function of V , D is the motor constant in m^3), J is the inertia momentum of the hydraulic motor shaft (in kg/m^2), L is the hydraulic motor shaft angular momentum (in kg/(m$^2 \cdot s$)), and S is the piston cross-sectional area (in m^2).

The accumulator pressure is captured with an isentropic model as [38]:

$$P_a(V) = \frac{P_{pr}}{(1 - \frac{V}{V_A})^\kappa} \tag{10}$$

where P_{pr} is the pre-charge pressure (in Pa), V_A is the total accumulator volume (in m^3), and κ is the specific heat ratio.

The dynamics of the generator shaft angular momentum are expressed in the second differential equation for the PTO as [38]

$$\dot{L} = D \cdot \eta_m \cdot P_a(V) - \frac{B}{J} \cdot L - T_G \tag{11}$$

in which η_m is the motor efficiency, B is the motor friction (in $N \cdot m \cdot s$) and T_G is the generator torque output (in $N \cdot m$).

With this dynamic model, the PTO force is a function of the accumulator volume and piston velocity as given by [38]

$$f_{PTO} = S \cdot P_a(V) + S \cdot k(S \cdot (\dot{x}_{ball} - \dot{x}_{hull}))) \tag{12}$$

where $k(S \cdot v)$ captures the pressure loss in a pipe due to friction under laminar conditions via the Haaland approximation of the Darcy equation given in Equation 13 [38].

$$\begin{aligned} & k(S \cdot (\dot{x}_{ball} - \dot{x}_{hull})) = \\ & \frac{K_s \cdot (L_g + L_{eq}) \cdot \rho_{hyd} \cdot S \cdot (\dot{x}_{ball} - \dot{x}_{hull})}{2Re \cdot D_h \cdot {A_p}^2} |S \cdot (\dot{x}_{ball} - \dot{x}_{hull})| \end{aligned} \tag{13}$$

K_S, L_g, L_{eq} and D_h are the pipe cross-section shape factor, geometric pipe length (in m), equivalent length of local resistance (in m) and hydraulic diameter of the pipe (in m^2), respectively. The term ρ_{hyd} represents the density of the hydraulic fluid (in kg/m^3) and A_p is the pipe cross-sectional area (in m^2) .

The radiation, buoyancy, drag and friction models are linked to the motion of the hull and the PTO force is a function of the relative motion between the hull and the ball. The resulting ten state model has the states [x_{ball} $\dot{x}_{ball}$ q_1 q_2 q_3 q_4 V L x_{hull} $\dot{x}_{hull}$] and the form:

$$
\begin{aligned}
\dot{x_1} = \;& x_2 \\
\dot{x_2} = \;& \tfrac{1}{M_{ball}}(-S_{rs}(x_1 - x_9) - f_{PTO}) \\
\dot{x_3} = \;& A_{r1} \cdot x_3 + A_{r2} \cdot x_4 + A_{r3} \cdot x_5 + A_{r4} \cdot x_6 + x_{10} \\
\dot{x_4} = \;& x_3 \\
\dot{x_5} = \;& x_4 \\
\dot{x_6} = \;& x_5 \\
\dot{x_7} = \;& -k_l h(x_7) - \tfrac{D}{J} x_8 + S(x_2 - x_{10}) \\
\dot{x_8} = \;& D\eta_m h(x_7) - \tfrac{B}{J} x_8 - T_G \\
\dot{x_9} = \;& x_{10} \\
\dot{x_{10}} = \;& \tfrac{1}{M_{hull} + m_{\infty,hull}}(-C_{r1} \cdot x_3 - C_{r2} \cdot x_4 \\
& -C_{r3} \cdot x_5 - C_{r4} \cdot x_6 + S_{rest} \cdot (x_1 - x_9) \\
& -\pi g {R_b}^2 \left(1 - \tfrac{|x_9|x_9}{3{R_b}^2}\right) x_9 \\
& -0.5\rho A_w C_d |x_{10} - v_f|(x_{10} - v_f) \\
& -F_n \mu_d tanh(\alpha x_{10}) - \mu_v x_{10} \\
& -F_n(\mu_s - \mu_d) e^{(-|x_{10}|/v_s)^2} tanh(\alpha x_{10}) \\
& + f_{ext} + f_{PTO})
\end{aligned}
\tag{14}
$$

The full nonlinear model was treated as the plant model while the MPC leveraged a linear version of the model. For the linear model, drag and friction are ignored and the buoyant force is linearized about a position of zero. The nonlinear PTO force (Equation 12) is a function of the accumulator volume and relative speed of the ball with respect to the hull. The PTO force was linearized about a the mid-point of the accumulator volume and a relative speed of zero. These assumptions make the model more easily for the MPC to leverage, but the linear model will carry with it errors depending on the state of the WEC.

B. Control Framework

The model was used with three different control frameworks in order to understand the combined influence of constraints and control structure on performance of each approach. The first control option considered was an optimally tuned passively damped system [42] and leveraged a control that computed the desired PTO force as proportional to the WEC velocity as illustrated in Fig. 3. Once the desired PTO force was calculated, the PTO model calculates the resulting flow entering the accumulator and the generator power output. This approach was treated as the base case. Additional control methods were explored for the base case including a reactive control approach, but this approach was unable to abide by all system constraints in some wave conditions. Leveraging reactive control can improve power production in the February wave conditions by up to 63% from the level achieved with passive damping only. However, the reactive control power output in February is still only 50% of that achieved with the reduced state linear MPC method discussed next. In the July conditions, reactive control is unable to produce significant power output without violating constraints. As such, the passive damping approach is shown as the base case here rather than the reactive control approach.

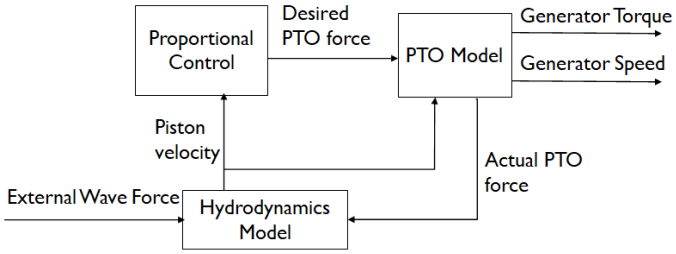

Fig. 3. Base Damped WEC PTO Control

Second, a linear MPC was used that included only the states associated with the hydrodynamics. This will be referred to as the reduced state linear MPC. With this approach, the control is based on a linearized model of states 1-6, 9 and 10. Using the hydrodynamics only allows a simpler MPC that is more computationally efficient to use but since the MPC has no knowledge

of the underlying PTO dynamics, it may be more limited in its ability to optimize. The reduced state linear MPC aims only to optimize the WEC motion so as to maximize the force entering into the PTO system. The MPC does this by seeking to maximize the velocity of the ball within the constraints of the hull in order to produce high forces on the hydraulic piston and into the hydraulic PTO system. The MPC is implemented using MATLAB's MPC toolbox with the continuous-time model structure and a controller sampling time of 0.05 seconds. The MPC uses a quadratic programming solver that uses the KWIK algorithm detail in [43]. The MPC outputs a desired PTO force and the PTO model is used to compute the actual PTO force achievable and translate this into a final generator torque and speed as shown in Fig. 4. The nonlinear model is used in the PTO and hydrodynamics (plant) model blocks.

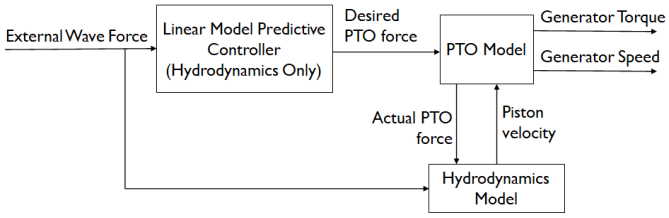

Fig. 4. Reduced State Linear MPC.

Third, an MPC was integrated which has full knowledge of the entire system dynamics including the PTO but which still leverages a linear model. For the full state linear MPC, the two DOF system will use a linearized version of its ten state model. The nonlinear terms related to the PTO dynamics in Eqs. (8) and (11) are also linearized. The resulting control structure is illustrated in Figure 5. The MPC predicts the torque that the PTO should output. This desired torque command is passed on the underlying PTO system. The PTO and hydrodynamics plant models are nonlinear.

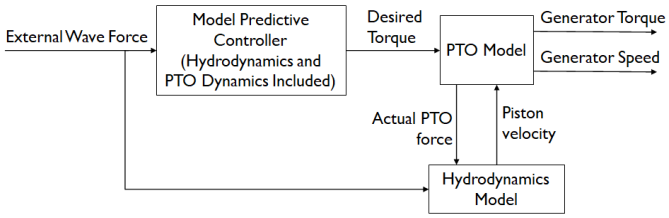

Fig. 5. Full State MPC.

Nonlinear MPC could also be used with the full nonlinear state space model. In prior work, the authors have used the same structure as in Fig. 5 for a simpler one DOF version of the system. However, this approach was computationally intensive and led to over-actuation of the underlying system [44].

C. System Constraints

The WEC system has limits on the PTO force that can be taken in by the hydraulic system given the sizing of the accumulator system and piping. Constraints are imposed to guarantee that the accumulator volume stays between its minimum and maximum and that the PTO force stays within limits in line with this sizing. Due to the structure of the TALOS device, it also has strict limits on the relative position of the mass and hull. The hull has a height of 3.2 m and the central mass must stay within this space and maintain a sufficient clearance from the hull in order to avoid damage to the PTO system. These constraints are included in the MPC formulation and ideally, it will solve for a solution that abides by all the constraints. However, at times, it is unable to find a solution that maintains both the position and PTO constraints.

D. Wave Prediction

MPC also requires a prediction of the upcoming wave state. Fusco and Ringwood demonstrated that energy capture was enhanced by utilizing a projection of the wave states into the future but the improvements ceased at some point depending on the size of the system and the time constant of its dominant pole [45]. This indicates that large devices (large radius) may require a longer prediction horizon. As such, accurate and relatively long predictions of wave forces may be needed as full scale devices are considered. In recent years, the prevalence of machine learning has enabled another option for predicting incoming wave features and prior work has shown that machine learning models are generally more accurate for short term predictions than physics-based models [46]. Structures such as multi-layer artificial neural networks have been successfully used along with MPC and shown to lead to significant improvements in performance particularly in conditions with irregular waves [47].

Prior work by the authors has illustrated that LSTM networks are able to accurately predict upcoming waves and as such, here the wave characteristics are assumed to be known. Wave characteristics were gathered for a location at a longitude of $8.5152°$W and latitude of $55.8919°$N (Figure 6). Characteristics were based on an analysis-forecast numerical wave model (product NORTH-WESTSHELF_ANALYSIS_FORECAST_WAV_004_014) from the Copernicus Marine Environment Monitoring Service (CMEMS).

The variation in key wave characteristics at this location were examined including significant wave height, energy wave period, zero-crossing mean wave period, peak period and mean wave direction. Data was available on an hourly basis. This hourly data was used to create higher resolution simulated data sets that represented the same significant wave height and peak period observed over the course of that hour. This allowed the control action to be examined with data that better reflects actual conditions. Significant wave height and peak period are focused on here as they directly impact the external wave force on the WEC and as such, will directly impact the control performance to be explored in the next section.

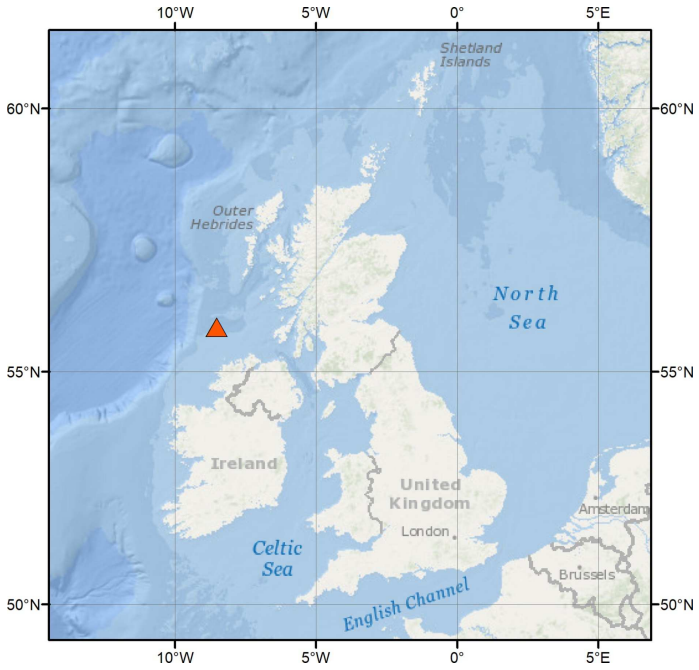

Fig. 6. Test site for wave data off the coasts of Ireland and Scotland

The measured wave statistics were recorded on an hourly basis and data for the 2021 year were used in this study. While hourly characteristics are useful for studies of the wave climate, control methodologies are implemented with a much smaller sampling time. In order to create a representative data set with the resolution needed for control development, these hourly wave characteristics were used to create a wave time series with a 0.05 second resolution that represent an irregular wave with the measured statistical significant wave height and peak period metrics. The wave time series was generated using Inverse Fourier transform from an assumed wave spectrum (Bretschneider) with the wave significant height, and peak period. As such the measurements along with the numerical model provide a prediction of the anticipated wave forces with respect to time at a resolution useful for control development. Average conditions for each month are laid out in Table I. Sea state conditions for the control evaluation were chosen to reflect the observed seasonal variation. February and July characteristics were selected since these captured the range of conditions observed. The resulting simulated irregular wave forces for the four conditions are shown in Figure 7.

III. Results

WEC performance for the three control options presented in Section II.B were tested initially keeping the prediction and control horizon constant at 5 sample periods and 1 sample period, respectively, for the MPC options. The performance was then evaluated for varying horizons. Prior work has shown that longer time horizons can improve power production but also lead to more aggressive control action [48].

A. Base Control Results

In the base control approach, the PTO force is simply proportional to the speed of the ball. The TALOS WEC has strict limits on the main mass location. If the desired PTO force will result in the ball coming too close to the hull, the flow to the accumulator and motor can be adjusted to create a PTO force that accommodates the constraints. Two other physical limitations

TABLE I
WAVE CHARACTERISTIC CONDITIONS

Month	Wave Height (m)	Peak Period (s)
January	3.02	11.49
February	3.88	12.07
March	3.36	11.84
April	2.24	10.78
May	2.11	10.16
June	2.08	9.52
July	1.26	8.82
August	1.55	8.88
September	2.25	10.08
October	2.98	10.42
November	3.82	11.28
December	3.70	12.25

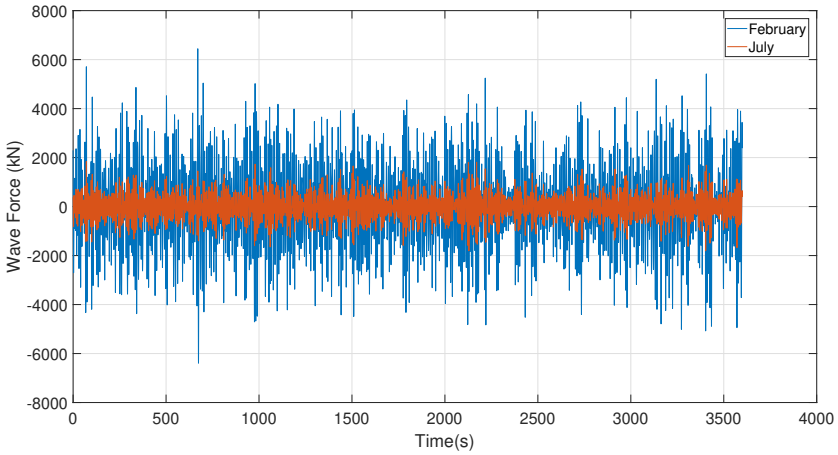

Fig. 7. External wave force for the four considered wave conditions

were incorporated: 1) the accumulator volume was required to be between zero and the maximum volume and 2) the PTO force must be within the limits achievable on the physical system. As illustrated in Fig. 8a, if no constraints are imposed the relative position between the ball and the hull quickly becomes negative meaning that in device like TALOS, damage will occur. This occurs quite quickly as seen in the Figure 8. In order to avoid the relative position moving to increasingly negative values, the proportional control action had to be reduced meaning the resulting PTO force and power output was also quite low (near 0kW) when no constraints are introduced. The July case shown in Figure 9 also encounters negative values. Only one minute is shown in the figures in order to allow the details of the trends to be examined. Once constraints are introduced the system is able to adjust the underlying PTO system to accommodate them. Two different constraints are introduced. The first only requires that the hull and ball do not touch (0m constraint) and the second requires a 0.1m distance between the two. Both constrained cases are able to produce high power output while abiding by the limits. As seen in subfigures b in Figures 8 and 9, the PTO forces undergo motions over the full allowable PTO motion and these motions are more frequent when higher constraints are introduced (0.1m vs 0m).

Power output fluctuates (subfigure c) but produces high amounts of power on average. When 0m constraints are present in the February case, 1.23MW of power are produced on average over the course of an hour. This is reduced to 948kW when constraints are integrated indicating that for this simple control approach the constraints can have a strong impact. This effect is similar in the July case where the power output is 349kW when no constraints are introduced, but improves to up to 1.5-1.56MW when constraints are present. Although there is more wave energy in February than July, the TALOS system as currently designed along with a simple control method is not able to capture the energy from the larger waves in February as well as it can capture the smaller motions in July. The larger motions increase the likelihood of constraint violation.

B. Reduced State MPC Results

The reduced state linear MPC aims to maximize the WEC velocity in order to optimize the power output. Since the eight-state model used includes only the hydrodynamics, the MPC has no knowledge of the underlying PTO dynamics and it cannot directly maximize the WEC power output. Instead, like the base case, it must choose the PTO force that produces the largest WEC motions and pass this PTO force command on to the PTO system. The PTO control then uses a feedforward method to

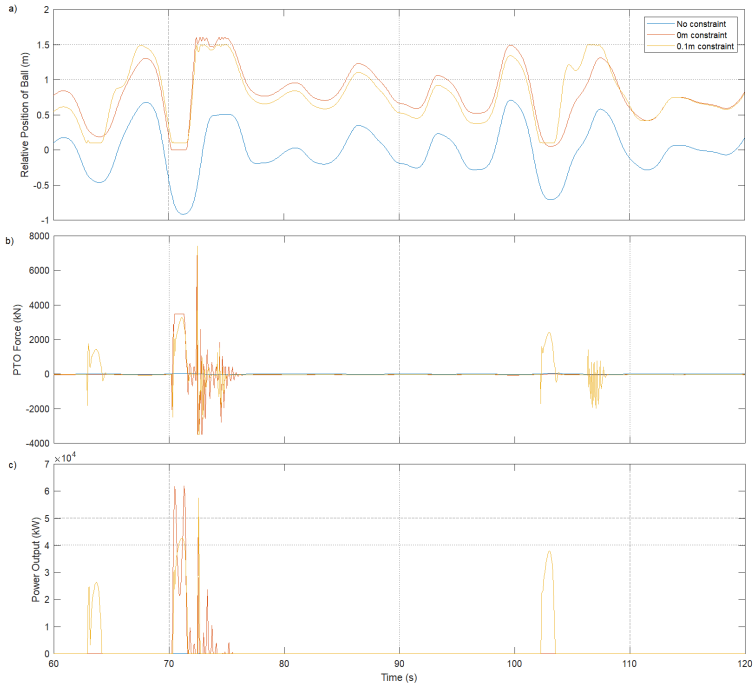

Fig. 8. a) Relative position between ball and hull, b) PTO force, and c) power output with baseline control and varying constraints with February wave conditions.

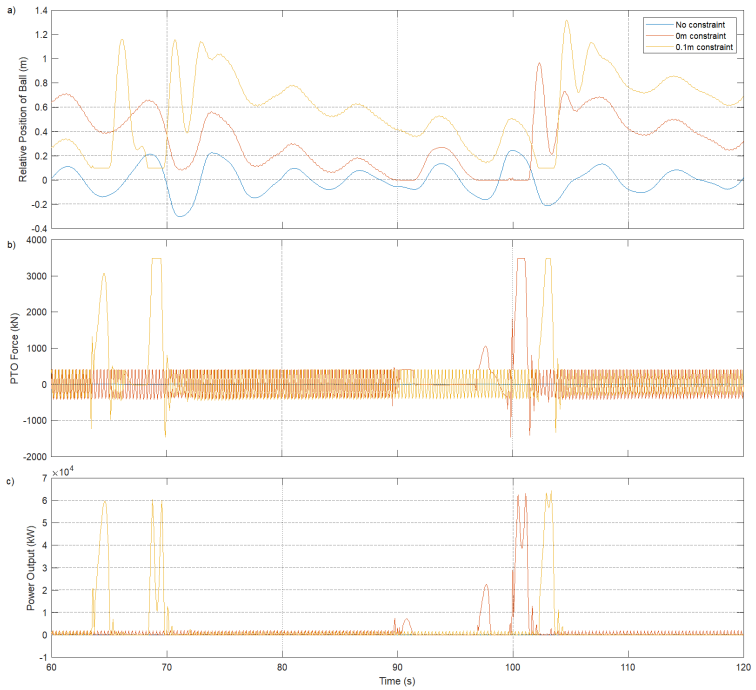

Fig. 9. a) Relative position between ball and hull, b) PTO force, and c) power output with baseline control and varying constraints with July wave conditions.

calculate the required generator torque needed to produce the desired PTO force based on the dynamics in Eqs. (9) and (11). Unlike the base case, the MPC options can base their decisions on a forecast of the upcoming wave which should, in theory, improve its outcome. However, the MPC also struggles without constraints. In the case with no constraints, the reduced state linear MPC quickly drives the ball towards the hull which would lead to damage and failure. Once constrained, the reduced state linear MPC is able to properly optimize and as illustrated in Fig. 10a, keeps the ball within the allowed range (0 to 1.6m) as in the base control method. Like the base controller, the reduced state linear MPC uses the PTO over the whole range of its motion, but with a very different PTO force profile. When no constraints are integrated the system clearly still would encounter

a collision of the ball and hull. When constraints are integrated, the power output is near 500kW in both cases illustrating poorer power production than the baseline case. This can be corrected by adjusting the prediction horizon.

At times when the system is nearing the constraint, the control action calls for smaller PTO forces (Figure 10b) that keep the central mass velocity low. When the MPC is able to largely maintain the constraint, it has larger control action resulting in larger velocities and power outputs. As seen in Figure 10c, the MPC with a 0.1m constraints exhibits a very different power output behavior. The PTO outputs power in a large sharp pulse rather than through smaller actions as in the unconstrained and 0m constraint cases (Figure 10d).

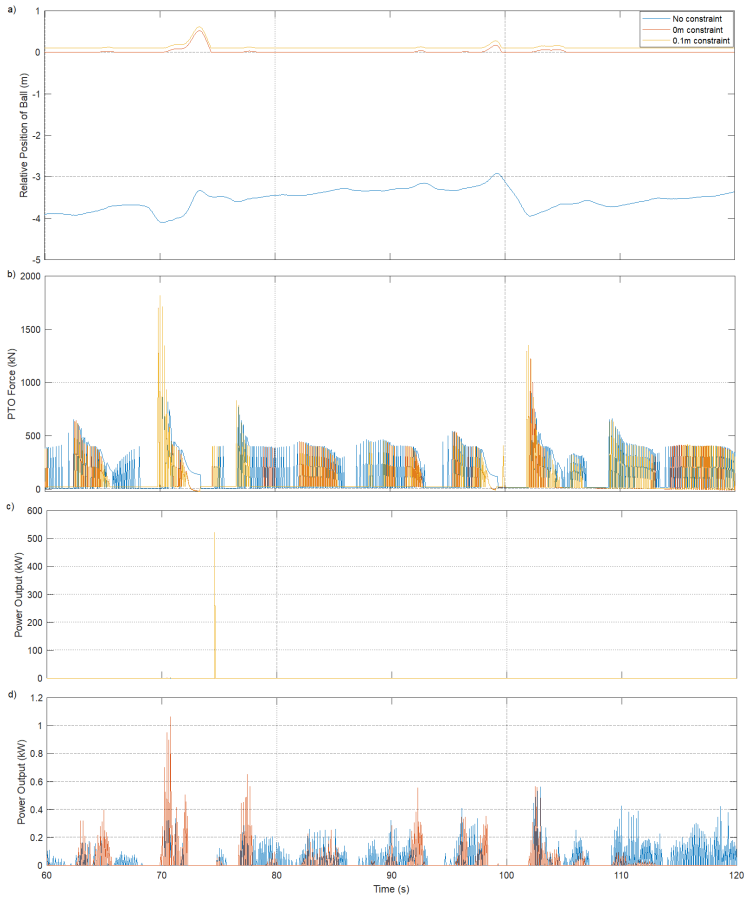

Fig. 10. a) Relative position between ball and hull, b) PTO force, and c) power output for 0.1m constraint and d)power output for the unconstrained and 0m constraint cases with the reduced state linear MPC and varying constraints with February wave conditions.

One critical factor for the MPC options is the prediction horizon over which it can optimize. A longer prediction horizon should allow the controller to better optimize power production, but will come at a computational price. The influence of the prediction horizon for the reduced state linear MPC option is shown in Figure 11. Increasing the prediction horizon improves the power output over 5 fold in the best case scenario. As such, the power output was able to be increased to 3MW in February and 2.6MW in July. The original horizon was 0.25s and the power output is normalized with respect to that horizon time. The prediction horizon of 1.75s results in the high power output output and extending the prediction horizon beyond 2s has a minimal and even negative impact on power output. This is likely due to the underlying linearization process used in this strategy. Increasing the control horizon did not have a sizable influence on the power output but increased the computational time and as such, was not examined further.

The July case exhibits some similar behavior to that of February with the unconstrained case producing more PTO force on average and higher power output. All options produce a fairly consistent PTO force and power output, but the actual output is low unless the horizon is increased as discussed previously. In the case with 0.1m constraints, the base control produces 948kW in February with the reduced MPC able to produce up to 3MW if the horizon is carefully chosen. Similarly, the base control is able to produce 1.5MW in July but the reduced MPC can produce 2.5MW indicating a clear advantage to using MPC as anticipated.

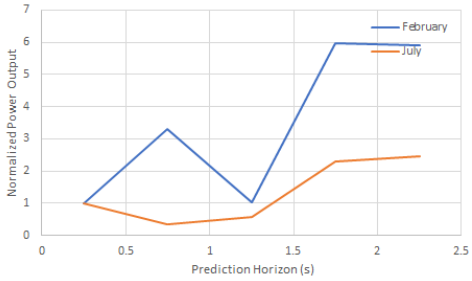

Fig. 11. Impact of prediction horizon on average power output for reduced state linear MPC.

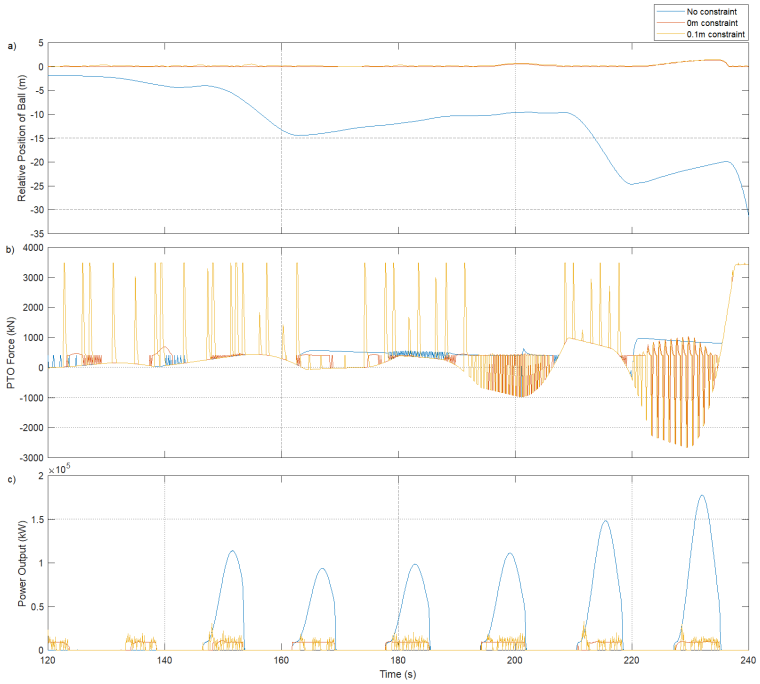

Fig. 12. a) Relative position between ball and hull, b) PTO force, and c) power output with the reduced state linear MPC and varying constraints with July wave conditions.

C. Full State MPC Results

Unlike the base and reduced state linear MPC options, the full state linear MPC is able to decide on its control action based on the WEC hydrodynamics as well as the underlying PTO dynamics. It is able to outperform the other methods, but requires proper weighting and constraints. Like the reduced state linear MPC, it will tend to drive the WEC main ball into the hull if position constraints are not imposed. It is also sensitive to output weighting. If the power output is not sufficiently weighted in the optimization, the system can tend to translate the motion of the mass into hydraulic fluid motion, driving fluid in and out of the accumulator without producing much power. If the weighting is increased, power output will improve significantly, but if the weight becomes too high, it can drive the PTO force to excessive levels. As such, constraints on position and PTO force and careful weighting are essential with this control option.

As illustrated in Fig. 13, the full state linear MPC has a periodic behavior with more conservative, but more constant PTO forces. The force is translated to a fairly periodic power output The power output is the highest of all the control options. When no constraints are integrated, the system produces 3.85MW in February. This drops to 1.6MW when constraints are introduced with a 0.25s prediction horizon but is able to be brought back to 3.7MW when the prediction horizon is lengthened. As such it produces 0.7MW more energy output (a 23% increase) compared to the reduced state option. As seen in Figure 14, similar behavior is also seen in July.

The full state linear MPC is strongly impacted by the prediction horizon as seen in Figure 15. A longer horizon improves the power output for both February and July but there is a larger benefit for February.

While the full state linear control provides improved power output, it is still basing its optimization on the linear model. Prior work has shown that improved performance should be feasible if the MPC is able to use the full nonlinear model for its calculation [44], but drives the PTO system through rapid fluctuations that may be problematic. The computational time also

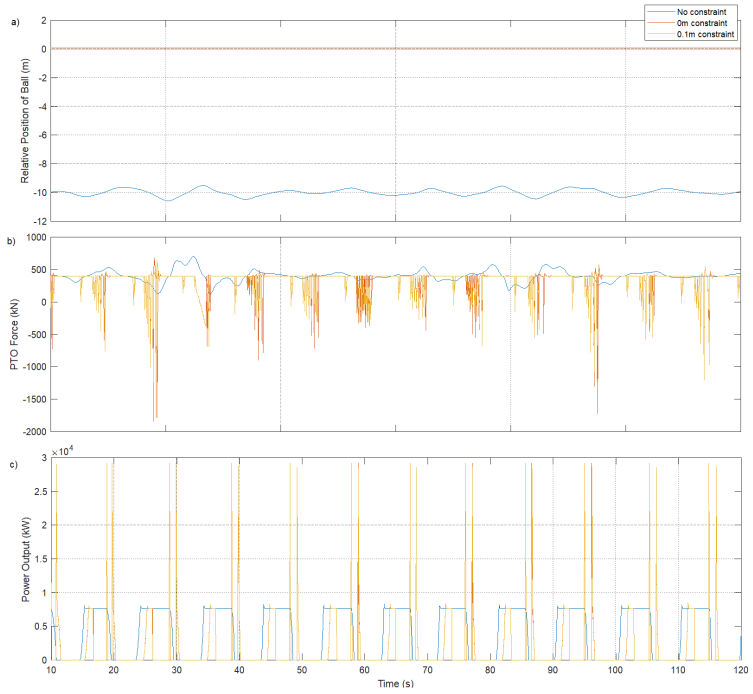

Fig. 13. a) Relative position between ball and hull, b) PTO force, and c) power output with the full state linear MPC and varying constraints with February wave conditions.

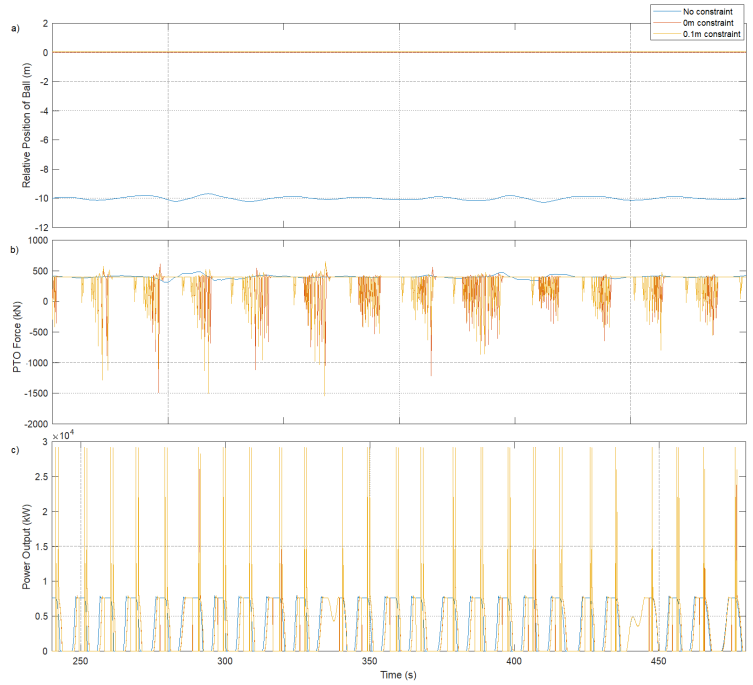

Fig. 14. a) Relative position between ball and hull, b) PTO force, and c) power output with the full state linear MPC and varying constraints with July wave conditions.

is limiting for the nonlinear MPC approach with computations taking over 100 times as long as the linear MPC approach.

IV. Conclusions and Future Work

In all three control cases considered, constraints are essential to proper operation. The key findings of this study were:

- Without position constraints, all control options produce forces that would send the central mass into the hull.

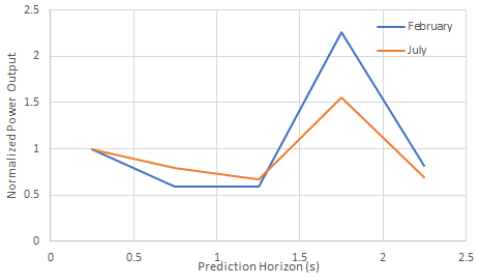

Fig. 15. Impact of prediction horizon on average power output for full state linear MPC.

- Once constraints are imposed, all MPC options are functional and perform better than the base control option. The reduced state linear version is only able to base its optimization on the linear hydrodynamics of the WEC and achieves an improvement over the base case with over three times the average power output.
- The full state MPC demonstrates a distinct improvement over the reduced state version with up to 23% more power output.
- Both the reduced state and full state MPC approaches benefit from a prediction time horizon of at least 2 seconds.
- The same control approaches function similarly in both summer and winter conditions but the winter case is more limited by the constraints.

Figure 16 illustrates the relative power output of the various control options.

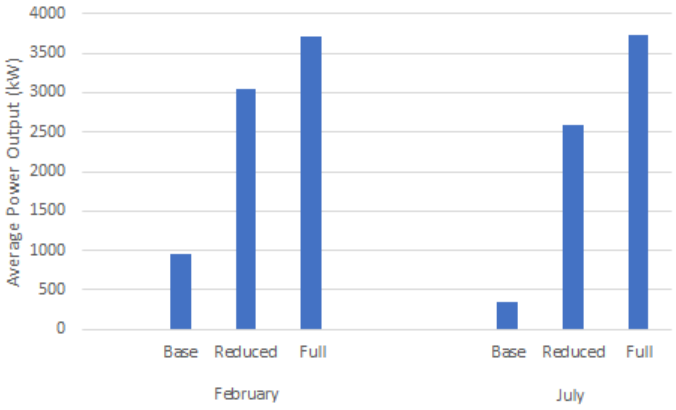

Fig. 16. Average power output for control options in February and July conditions. Results for the reduced and full state MPC are for the optimized prediction horizon

This study illustrates that abiding by all the constraints in the heave direction is challenging in an enclosed WEC design with an inertial mass PTO and if constraints over the six DOF of TALOS are to be considered, balancing the computational complexity of the control with performance will likely be difficult. The results indicate that full state MPC may be the best pathway forward. In order to manage computation time, there may be benefits to leveraging machine learning for control. Future work will examine multi-axis control, examine different mooring designs, and investigate the influence of the uncertainty of the wave predictions on controller effectiveness in the full six degrees of freedom.

V. Acknowledgments

This work was partially supported by the US-UK Fulbright Commission through the Fulbright-Lancaster University Scholar Award 2022-2023. Additional funding was provided by the UK Engineering and Physical Sciences Research Council (EPSRC grant number EP/V040561/1) for the project Novel High-Performance Wave Energy Converters with advanced control, reliability and survivability systems through machine-learning forecasting (NHP-WEC).

References

[1] Ringwood, J. V., Bacelli, G., and Fusco, F., 2014. "Energy-maximizing control of wave-energy converters: The development of control system technology to optimize their operation". *IEEE control systems magazine,* **34**(5), pp. 30–55.
[2] Aderinto, T., and Li, H., 2018. "Ocean wave energy converters: Status and challenges". *Energies,* **11**(5).
[3] Huang, S., Shi, H., Cao, F., Tan, J., Cheng, H., Li, D., Liu, S., Gong, H., and Tao, J., 2019. "Experimental study on interaction between degrees of freedom in a wave buoy". *Journal of Ocean University of China,* **18**, pp. 1256–1264.

[4] Parker, R. P. M., Harrison, G., and Chick, J., 2007. "Energy and carbon audit of an offshore wave energy converter". *Proceedings of the Institution of Mechanical Engineers, Part A: Journal of Power and Energy,* **221**(8), pp. 1119–1130.

[5] Aggidis, G., and Taylor, C., 2017. "Overview of wave energy converter devices and the development of a new multi-axis laboratory prototype". *IFAC-PapersOnLine,* **50**(1), pp. 15651–15656.

[6] "Têtu, Amélie", P. A., and Kofoed, J. P. *Power Take-Off Systems for WECs*.

[7] Hals, J., Falnes, J., and Moan, T., 2011. "A Comparison of Selected Strategies for Adaptive Control of Wave Energy Converters". *Journal of Offshore Mechanics and Arctic Engineering,* **133**(3), 03. 031101.

[8] García-Violini, D., Faedo, N., Jaramillo-Lopez, F., and Ringwood, J. V., 2020. "Simple controllers for wave energy devices compared". *Journal of Marine Science and Engineering,* **8**(10), p. 793.

[9] Hals, J., Falnes, J., and Moan, T., 2011. "Constrained optimal control of a heaving buoy wave-energy converter". *Journal of Offshore Mechanics and Arctic Engineering,* **133**(1).

[10] Li, G., and Belmont, M. R., 2014. "Model predictive control of sea wave energy converters–part i: A convex approach for the case of a single device". *Renewable Energy,* **69**, pp. 453–463.

[11] Genest, R., and Ringwood, J. V., 2016. "Receding horizon pseudospectral control for energy maximization with application to wave energy devices". *IEEE Transactions on Control Systems Technology,* **25**(1), pp. 29–38.

[12] Garcia-Violini, D., and Ringwood, J. V., 2021. "Energy maximising robust control for spectral and pseudospectral methods with application to wave energy systems". *International Journal of Control,* **94**(4), pp. 1102–1113.

[13] Li, G., 2017. "Nonlinear model predictive control of a wave energy converter based on differential flatness parameterisation". *International Journal of Control,* **90**(1), pp. 68–77.

[14] Faedo, N., García-Violini, D., Scarciotti, G., Astolfi, A., and Ringwood, J. V., 2019. "Robust moment-based energy-maximising optimal control of wave energy converters". In 2019 IEEE 58th Conference on Decision and Control (CDC), IEEE, pp. 4286–4291.

[15] Faedo, N., Scarciotti, G., Astolfi, A., and Ringwood, J. V., 2021. "Nonlinear energy-maximizing optimal control of wave energy systems: A moment-based approach". *IEEE Transactions on Control Systems Technology,* **29**(6), pp. 2533–2547.

[16] Ringwood, J. V., 2020. "Wave energy control: status and perspectives 2020". *IFAC-PapersOnLine,* **53**(2), pp. 12271–12282.

[17] Jama, M., Mon, B. F., Wahyudie, A., and Mekhilef, S., 2021. "Maximum energy capturing approach for heaving wave energy converters using an estimator-based finite control set model predictive control". *IEEE Access,* **9**, pp. 67648–67659.

[18] Tona, P., Sabiron, G., and Nguyen, H.-N., 2019. "An energy-maximising mpc solution to the wec control competition". In International Conference on Offshore Mechanics and Arctic Engineering, Vol. 58899, American Society of Mechanical Engineers, p. V010T09A034.

[19] Ling, B. A., Bosma, B., and Brekken, T. K., 2019. "Experimental validation of model predictive control applied to the azura wave energy converter". *IEEE Transactions on Sustainable Energy,* **11**(4), pp. 2284–2293.

[20] Penalba, M., and Ringwood, J. V., 2019. "Linearisation-based nonlinearity measures for wave-to-wire models in wave energy". *Ocean Engineering,* **171**, pp. 496–504.

[21] Haider, A. S., Brekken, T. K. A., and McCall, A., 2021. "Real-time nonlinear model predictive controller for multiple degrees of freedom wave energy converters with non-ideal power take-off". *Journal of Marine Science and Engineering,* **9**(8).

[22] Faedo, N., Olaya, S., and Ringwood, J. V., 2017. "Optimal control, mpc and mpc-like algorithms for wave energy systems: An overview". *IFAC Journal of Systems and Control,* **1**, pp. 37–56.

[23] Cavaglieri, D., Bewley, T. R., and Previsic, M., 2015. "Model predictive control leveraging ensemble kalman forecasting for optimal power take-off in wave energy conversion systems". In 2015 American Control Conference (ACC), pp. 5224–5230.

[24] Zhan, S., Na, J., Li, G., and Wang, B., 2020. "Adaptive model predictive control of wave energy converters". *IEEE Transactions on Sustainable Energy,* **11**(1), pp. 229–238.

[25] Mérigaud, A., and Ringwood, J. V., 2018. "Towards realistic non-linear receding-horizon spectral control of wave energy converters". *Control Engineering Practice,* **81**, pp. 145–161.

[26] Brekken, T. K., 2011. "On model predictive control for a point absorber wave energy converter". In 2011 IEEE Trondheim PowerTech, pp. 1–8.

[27] Bracco, G., Canale, M., and Cerone, V., 2020. "Optimizing energy production of an inertial sea wave energy converter via model predictive control". *Control Engineering Practice,* **96**, p. 104299.

[28] Jama, M., Wahyudie, A., Assi, A., and Noura, H., 2014. "Function-based model predictive control approach for maximum power capture of heaving wave energy converters". In *ICREGA'14-Renewable Energy: Generation and Applications*. Springer, pp. 299–313.

[29] Hendrikx, R. W. M., Leth, J., Andersen, P., and Heemels, W. P. M. H., 2017. "Optimal control of a wave energy converter". In 2017 IEEE Conference on Control Technology and Applications (CCTA), pp. 779–786.

[30] Zhan, S., Li, G., and Bailey, C., 2019. "Economic feedback model predictive control of wave energy converters". *IEEE Transactions on Industrial Electronics,* **67**(5), pp. 3932–3943.

[31] Bacelli, G., and Ringwood, J. V., 2013. "A geometric tool for the analysis of position and force constraints in wave energy converters". *Ocean Engineering,* **65**, pp. 10–18.

[32] Sergiienko, N. Y., Bacelli, G., Coe, R. G., and Cazzolato, B. S., 2022. "A comparison of efficiency-aware model-predictive control approaches for wave energy devices". *Journal of Ocean Engineering and Marine Energy,* **8**(1), pp. 17–29.

[33] Kovaltchouk, T., Rongère, F., Primot, M., Aubry, J., Ahmed, H. B., and Multon, B., 2015. "Model predictive control of a direct wave energy converter constrained by the electrical chain using an energetic approach". In European Wave and Tidal Energy Conference 2015.

[34] Karthikeyan, A., Previsic, M., Scruggs, J., and Chertok, A., 2019. "Non-linear model predictive control of wave energy converters with realistic power take-off configurations and loss model". In 2019 IEEE Conference on Control Technology and Applications (CCTA), pp. 270–277.

[35] Bacelli, G., Genest, R., and Ringwood, J., 2015. "Nonlinear control of flap-type wave energy converter with a non-ideal power take-off system". *Annual Reviews in Control,* **40**, pp. 116–126.

[36] Mérigaud, A., and Tona, P., 2020. "Spectral control of wave energy converters with non-ideal power take-off systems". *Journal of Marine Science and Engineering,* **8**(11), p. 851.

[37] Duarte, T., Sarmento, A., Alves, M., and Jonkman, J., 2013. State-space realization of the wave-radiation force within fast. Tech. rep., National Renewable Energy Lab.(NREL), Golden, CO (United States).

[38] Bacelli, G., Gilloteaux, J.-c., and Ringwood, J., 2008. "State space model of a hydraulic power take off unit for wave energy conversion employing bondgraphs". *Proc. World Renewable Energy Conference, Glasgow*, 01.

[39] Richter, M., Magaña, M. E., Sawodny, O., and Brekken, T. K., 2014. "Power optimisation of a point absorber wave energy converter by means of linear model predictive control". *IET Renewable Power Generation,* **8**(2), pp. 203–215.

[40] Zhan, S., He, W., and Li, G., 2017. "Robust feedback model predictive control of sea wave energy converters". *IFAC-PapersOnLine,* **50**(1), pp. 141–146. 20th IFAC World Congress.

[41] Zhang, Y., and Li, G., 2022. "Robust tube-based model predictive control for wave energy converters". *IEEE Transactions on Sustainable Energy*, pp. 1–9.

[42] Maria-Arenas, A., Garrido, A. J., Rusu, E., and Garrido, I., 2019. "Control strategies applied to wave energy converters: State of the art". *Energies,* **12**(16), p. 3115.

[43] Schmid, C., and Biegler, L. T., 1994. "Quadratic programming methods for reduced hessian sqp". *Computers & chemical engineering,* **18**(9), pp. 817–832.

[44] Hall, C., Wu, Y., Sheng, W., and Aggidis, G., 2023. "The impact of control structure and constraints on the performance of a wave energy converter with a hydraulic pto system". In 2023 International Society of Offshore and Polar Engineers (ISOPE) Confernece.
[45] Fusco, F., and Ringwood, J. V., 2012. "A study of the prediction requirements in real-time control of wave energy converters". *IEEE Transactions on Sustainable Energy,* **3**(1), pp. 176–184.
[46] Reikard, G., Pinson, P., and Bidlot, J.-R., 2011. "Forecasting ocean wave energy: The ecmwf wave model and time series methods". *Ocean Engineering,* **38**(10), pp. 1089–1099.
[47] Li, L., Gao, Y., Ning, D., and Yuan, Z., 2021. "Development of a constraint non-causal wave energy control algorithm based on artificial intelligence". *Renewable and Sustainable Energy Reviews,* **138**, p. 110519.
[48] Sergiienko, N. Y., Cocho, M., Cazzolato, B. S., and Pichard, A., 2021. "Effect of a model predictive control on the design of a power take-off system for wave energy converters". *Applied Ocean Research,* **115**, p. 102836.